EFDA–JET–PR(11)56

C. Perez von Thun, A. Salmi, A. Perona, S.E. Sharapov, S.D. Pinches,
S. Popovichev, S. Conroy, V.G. Kiptily, M. Brix, M. Cecconello, T. Johnson
and JET EFDA contributors

Study of Fast Ion Transport Induced by Fishbones on JET

Study of Fast Ion Transport Induced by Fishbones on JET

C. Perez von Thun[1,2], A. Salmi[3], A. Perona[4], S.E. Sharapov[5], S.D. Pinches[5], S. Popovichev[5], S. Conroy[6], V.G. Kiptily[5], M. Brix[5], M. Cecconello[6], T. Johnson[7] and JET EFDA contributors*

JET-EFDA, Culham Science Centre, OX14 3DB, Abingdon, UK

[1]Max-Planck-Institut für Plasmaphysik, EURATOM-Association IPP, Garching, D-85748, Germany
[2]JET-EFDA Close Support Unit, Culham Science Centre OX14 3DB, Abingdon, UK
[3]Association EURATOM-Tekes, Aalto University, Department of Applied Physics, Finland
[4]Centre for Fusion, Space and Astrophysics, Department of Physics, University of Warwick, Coventry CV4 7AL, UK
[5]EURATOM-CCFE Fusion Association, Culham Science Centre, OX14 3DB, Abingdon, OXON, UK
[6]EURATOM-VR Association, Department of Physics and Astronomy, Uppsala University, 75120 Uppsala, Sweden
[7]EURATOM-VR Association, Fusion Plasma Physics, EES, KTH, 10044 Stockholm, Sweden
** See annex of F. Romanelli et al, "Overview of JET Results", (23rd IAEA Fusion Energy Conference, Daejon, Republic of Korea (2010)).*

Preprint of Paper to be submitted for publication in
Nuclear Fusion

ABSTRACT.
The impact of fishbone oscillations onto a confined fast ion population is simulated for a JET plasma and benchmarked against experiment with the help of neutron rate measurements. The transient drops in volume integrated neutron emission are found to be mainly caused by a redistribution of the confined ion population rather than fast ion loss. The simulations yield a quadratic dependence of the neutron drop on the fishbone amplitude (rather than the linear dependence expected from mode particle pumping theory), which is indicative of fast ion stochastic orbit diffusion dominating over convective transport processes. It is found that the simulations are able to correctly reproduce the magnitude of the experimentally observed drop in volume integrated neutron emission to within a factor 2.

1. INTRODUCTION

MHD instabilities driven unstable in the presence of a fast (i.e. suprathermal) ion population may, at sufficiently high amplitude, lead to unacceptably high fast ion transport in ITER and other burning plasma experiments (with consequences to the plasma performance or the first wall integrity [1, 2]). While a number of mechanisms for accelerated transport of fast ions in the presence of a perturbation field have been identified and are well established theoretically, there have been relatively few quantitative comparisons of experimental measurements with theory. For the case of Alfven Eigenmodes (AEs) [3–6], quantitative comparisons between the measured fluctuation levels and the expected transport were first presented in [7, 8] and more recently and with state of the the art diagnostics in [9]. In all three cases it was found that calculations with measured mode amplitudes significantly underestimate the observed fast ion transport and that a reasonable match was only reached after increasing the mode amplitude artificially by an order of magnitude. Recently, it was found that the discrepancy in [8] could be explained by the non-linear generation of an n = 0 harmonic of the TAE perturbation [10], while the discrepancy in [9] was found to stem from the omission of the electrostatic potential associated with the AE magnetic perturbation [11, 12]. After inclusion of this effect a satisfactory agreement with experiment could be obtained. Here we try to make an analogous quantitative assessment for a different type of fast ion driven instability, the fishbone oscillation. First identified and studied in detail on PDX and PBX [13–18], and subsequently reported on many other tokamaks (including JET [19–21]), it is widely accepted that this type of oscillation is excited through the resonant interaction of a fast ion population in the plasma with the internal kink mode [22, 23]. The reference quantity used here to compare the theoretically predicted amount of fast ion transport against experiment will be the drop in 2.5MeV neutron emission (from D-D fusion reactions) induced by the fishbone. The paper is structured as follows. Section 2 presents a brief characterisation of the discharge to be analysed and the overall simulation strategy. The outcome of these simulations and most importantly its benchmarking against the experimental neutron measurements is described in section 3. In the final section conclusions are drawn.

2. EXPERIMENTAL OBSERVATIONS AND SIMULATION SETUP

To carry out this assessment JET Pulse No: 69100 has been chosen. This is a well diagnosed discharge that has been previously documented for the study of fishbonerelated fast ion losses with a scintillator probe detector [24, 25]. The main discharge characteristics and experimental findings are repeated below for convenience, for further details the reader is referred to [24].

Pulse No: 69100 is an ELMy H-mode discharge with conventional (fully relaxed) qprofile. During its flat top the discharge parameters are as follows: $B = 2.7T$, $I_p = 1.2MA$, edge safety factor $q_{95} \sim 6.5$, normalised beta $\beta_N = 2.6$, poloidal beta $\beta_{pol} = 1.8$, Greenwald fraction $n_e/n_{GW} = 0.77$, triangularity $\delta \sim 0.4$. The plasma is composed of 95 percent deuterium and 5 percent hydrogen (inferred from visible spectroscopy measurements at the plasma boundary). The auxiliary heating (figure 1a) consists of 15MW of co-NBI (deuterium, max. 130keV injection energy) and 6MW of coupled ICRH (42MHz, giving for the hydrogen minority a central resonance position 28cm inboard of the magnetic axis). The Neutral Particle Analyser (NPA) and gamma-ray spectrometer diagnostics show negligible second harmonic deuterium acceleration, which is in agreement with both PION [26] and SELFO [27] simulations.

The MHD activity in this pulse is composed of fishbones and sawteeth in the plasma core, and small ELMs at the plasma boundary. The time interval where fishbones occur is highlighted in figure 1a. The fishbones themselves are driven unstable by the fast neutral beam injected deuterons and not by the RF accelerated protons, as the fishbone activity was equally seen in a separate RF-free reference discharge [24]. Also, in Pulse No: 69100 the fishbone activity starts 400ms before the ICRF heating is switched on and disappears following the ramp down in neutral beam power, well before the ICRH is switched off (the last fishbone is observed at t = 23.92s, whereas the ICRH power flat top lasts until 24.10s).

Of the three ^{235}U fission chambers that are routinely used on JET to measure the neutron emission from the plasma, one is connected to a fast logarithmic ADC (250kHz sampling). Once linearised (neglecting the bleed current from the detector), smoothed and cross-calibrated against the slower neutron signal from the three fission chambers, this signal is shown in figure 1b for a time window with fishbones. Temporary drops in neutron emission of mild amplitude (few percent) are visible which are clearly correlated with the fishbone bursts and whose reproduction in simulations will be attempted here. In this discharge the neutron production is dominated by the beam contribution (according to TRANSP [28], 95% of the neutrons originate from either beam-target or beam-beam reactions, whereas the RF accelerated protons do not directly contribute to the neutron rate), hence the neutron emission drop must originate from a partial redistribution and/or loss of the NBI slowing down distribution.

To determine whether the measured fishbone activity can explain the observed fast-ion transport (drop in neutron emission), a fast ion distribution has been followed in the Hamiltonian guiding centre code HAGIS [29,30] (release 10.06) using a time dependent 3-D magnetic configuration. This configuration has been constructed by superimposing the perturbation field of an internal kink

mode (whose radial eigenfunction is a good approximation for the fishbone) to the axisymmetric equilibrium constructed by EFIT (where the q = 1 rational surface position has been validated with sawtooth inversion radius measurements [31]). Here, the radial eigenfunctions are computed by the linear MHD code MISHKA-1 [32], which solves the ideal incompressible MHD equations. To reproduce a typical fishbone cycle, the obtained eigenfunctions are scaled with a time dependent amplitude and frequency that match the experimentally observed values, using the same procedure as in [24, 25]. The amplitude is specified through a third order polynomial as follows. For $t \leq t_{sat}$:

$$\frac{A(t)}{A_{sat}} = \frac{t^2}{t_{sat}^3}(3t_{sat} - 2t) \tag{1}$$

whereas for $t_{sat} < t \leq t_{period}$:

$$\frac{A(t)}{A_{sat}} = (t_{period} - t)^2 \frac{[3(t_{period} - t_{sat}) - 2(t_{period} - t)]}{(t_{period} - t_{sat})^3} \tag{2}$$

where $A \equiv \delta B_r/B_0$ is the radial perturbation amplitude (normalised to the magnetic field on axis), t_{sat} is the time at which the maximum fishbone amplitude, A_{sat}, is reached, and tperiod is the total duration of the fishbone. The waveform appearance is illustrated in figure 2. In what concerns the wave frequency, it decreases linearly in time over the fishbone period. Hence, for each fishbone there are four parameters to be linked to experiment: (i) the saturation amplitude Asat, (ii) the duration t_{period}, (iii) the initial wave frequency value and (iv) the rate at which the wave frequency decreases. (ii) and (iv) were inferred from magnetic fluctuation measurements and were taken to be 11 ms and $-0.454 \cdot 10^6$ Hz/s, respectively. (iii) was inferred from magnetic fluctuation measurements and CXRS measurements near the q = 1 rational surface (needed to substract the rotation frequency of the background plasma) and determined to be 7 kHz. (i) was obtained by matching magnetic flux surface displacements inside q = 1 (visualized through Poincare plots of magnetic field lines in the 3-D perturbed equilibrium) to electron temperature profile displacements at the time of maximum fishbone amplitude measured with an array of ECE radiometers. The electron temperature profile displacements are in turn obtained using the expression

$$\xi = \frac{\delta T_e}{|\nabla T_e|} \tag{3}$$

which neglects plasma compressibility [33]. Asat is the only quantity that was found to vary more strongly from fishbone to fishbone and hence a scan was performed to cover the full range of observed values ($2.5 \cdot 10^{-3}$ - $1.5 \cdot 10^{-2}$).

The initial beam ion distribution to be followed in HAGIS was computed by the guiding centre following Monte Carlo code ASCOT [34] with neo-classical fast ion transport. This pre-fishbone distribution was taken to be the stationary NBI slowing down distribution for the flat top phase of Pulse No: 69100, i.e. it is assumed that after a fishbone burst the fast ion distribution is able to fully

recover before the next fishbone is triggered. The ensemble was composed of 635.000 markers with variable weights, representing a total population of $1.0^4 \cdot 10^{20}$ fast deuterons. Sliced in radial intervals, its dependency on the orbit-invariants energy and $\Lambda = \mu_m B_0/E = B_0(1 - \cos^2 \vartheta_p)/B$ (where μ_m is the magnetic moment, B_0 is the magnetic field on axis, E is the energy, and ϑ_p is the pitch angle) is depicted in figures 3a and b, respectively. In figure 3a, the two main "steps" are due to the fact that some of the beam sources were injecting at energies 110-130keV while others were injecting at 71-76keV. On the outermost curve ($0.8 < s < 1$) two smaller steps are visible which correspond to the half energy fractions of those two groups. These are no longer visible when moving deeper into the plasma due to the limited beam penetration depth at lower energies. For computational reasons, slowing down ions were not followed down all the way to thermalisation (where they effectively no longer contribute to the neutron rate), which is why the distribution function is seen to decrease at low energies. Although all neutral beam sources are co-injected into the plasma, a non-negligible fraction of the fast ion population ends up on counter-passing orbits through pitch angle scattering. Ignoring exotic orbit types, the orbit mix is found to be as follows: 48.2 % of fast ions are co-passing, 33.9 % are trapped, 17.8 % are counter-passing.

Figure 3c shows the resulting steady-state neutron rate which ASCOT predicts for this distribution, together with the experimentally measured neutron signal. Both are consistent with each other so the ASCOT distribution clearly is in the right ballpark. Note that the two do not necessarily have to agree, as ASCOT does not know about MHD modes in the plasma. The fact that they do agree nonetheless suggests that in this discharge the impact of fishbones is only transient, in other words, the classically predicted fast ion distribution is recovered prior to the next fishbone (thus supporting the above assumption). At the same time it is worth emphasizing that in this work we are mainly interested in relative changes to the neutron emission, rather than in its absolute value, so for our purposes an absolute agreement between the two is not essential.

This completes the description of the simulation setup. In the next section, the results from the fishbone simulations will be presented and the resulting neutron rate will be re-evaluated.

3. RESULTS

Figure 4 shows a series of plots in which the computed pre- and post-fishbone distributions are compared for a selection of four fishbones with different size ($A_{sat} = 2.5 \cdot 10^{-3}$, $5.0 \cdot 10^{-3}$, $1.0 \cdot 10^{-2}$, $1.25 \cdot 10^{-2}$). It can be seen that the main feature is a reduction in fast ion density inside $q = 1$ and a slight increase outside $q = 1$. Likewise, the radial profile of neutron emission (not shown here) displays an analogous behaviour. This feature gets accentuated with increasing fishbone amplitude. Due to the finite peaking of the background plasma density profile (for this discharge, $n_e(s = 0.1)/n_e(s = 0.5) = 1.18$), and as the neutron production is dominated by beam-target reactions, the broadening of the fast ion profile can be expected to lead to an overall "instantaneous" (the fishbone duration is short relative to the slowing down time of beam ions) reduction of the volume integrated neutron rate. Also, very close to the plasma edge there is a large relative decrease in

fast ion density (bottom row) which is due to the loss of marginally confined ions. However, as the absolute fast ion density is much lower near the plasma boundary, this effect turns out to be relatively unimportant. The fast ion redistribution effect is dominant over the losses, with the latter contributing not more than 10% to the total neutron rate drop (this is in contrast to the case of PDX [14], where, due to the smaller device dimensions and plasma current, losses were most likely the dominant factor).

For each ion, the fishbone induced radial displacement will depend on the particular orbit topology, the resonance closeness to the perturbation wave-field as well as on non-resonant wave-particle interaction processes. Further insight into the redistribution physics can be obtained by evaluating the proximity to wave-particle resonance for each of the ions and the associated radial displacement. The resonance condition for energetic ions to interact with a wave field is $n\omega_\phi - p\omega_\theta - \omega_\phi = 0$ [35], where n is the toroidal mode number (= 1), $p \in \mathbb{Z}$, ω_ϕ is the toroidal ion transit frequency, ω_θ is the poloidal ion transit frequency (in the case of trapped particles, the poloidal bounce frequency) and ω is the wave frequency. The above formula is valid for both trapped and passing ions. By defining the resonance parameter $\Omega_{np} \equiv (n\omega_\phi - p\omega_\theta - \omega)/2\pi$, the proximity to the resonance condition has been evaluated for each ion in the fast ion distribution by inserting for ω_ϕ and ω_θ the original (unperturbed) value (i.e. neglecting variations in ω_ϕ and ω_θ during the fishbone) and maximising the value of $1/\Omega_{np}$ by scanning ω and p (in the range $2 \le \omega/2\pi \le 7$kHz in steps of 100Hz, and $|p| \le 100$, respectively). ω_ϕ and ω_θ were obtained by following ions over a long enough time interval (with the fishbone perturbation switched off) so as to average over several orbits. Note here that the initial beam distribution provided by the ASCOT code had no "mesh accumulation" for launching ions near expected resonances. Figure 5a plots the distribution of fast ions in terms of (the logarithm of) $1/\Omega_{np}$. A deeply negative abscissa value implies that orbits are far away from resonance with the fishbone wave. It can be seen that the distribution is double-peaked, with the peak near –4 (i.e. resonance $\sim 10^4$Hz away) originating mainly from co-passing fast ions, whereas for the second peak near –2 (better resonance match, to within $\sim 10^2$Hz) about two thirds of ions are trapped, with the remainder composed of either co- or counter-passing ions. The choice of step size used for the frequency scan (here: 100Hz) has some influence on the precise location of the latter peak, but the double peak structure always persists. The average displacement experienced by ions versus resonance proximity is given in figure 5b. A priori one would expect that only ions close to resonance experience significant radial redistribution. On the contrary, efficient redistribution is observed over a surprisingly wide range. The amount of displacement remains almost flat between –3 and 0 and the transition to negligible displacement only takes place between –4 and –3.[§] The highest displacements occur above 0, but in practice these are unimportant as very few ions are that close to resonance (the raggedness also increases here due to the poorer statistics). Combining the two plots, i.e. multiplying the number of ions with the average displacement per ion at each

[§] *This coincides roughly with the transition in the orbit mix from predominantly trapped to co-passing particles, as shown underneath subfigure (a)). However, it is erroneous to assume that co-passing particles are not disturbed by the fishbone, as demonstrated by the orbit example on the right hand side.*

resonance level, yields the plot in figure 5c. The main conclusion here is that, due to the resonance broadening effect, the peak that was nominally far away from resonance still contributes roughly as much to the overall fast ion redistribution as the peak close to resonance, hence the importance of using the full beam distribution for this type of studies.

There are mainly two reasons for this resonance broadening. First, the finite growth (and decay) rate of the fishbone leads to a broadening of the frequency interval which is effective for interaction. For the fishbones under consideration in this discharge, the growth rate is of order 3000 s−1 and the decay rate of order $300s^{-1}$. Secondly, it turns out to be oversimplifying to consider ω_ϕ and ω_θ as fixed numbers for each ion, as ω_ϕ and ω_θ change dynamically throughout an orbit (velocities are different on the low than on the high field side, etc), and these dynamic variations are of order kHz, too (e.g. for the co-passing ion example depicted on the left hand side of figure 5, the "instantaneous" $\omega_\phi/2\pi$ varies periodically between 70 and 76 kHz). On the contrary, the nonlinear modification of ω_ϕ and ω_θ by the fishbone (which may in turn bring the ions into resonance) seems not to be important ($\omega_\phi$and ω_θ are only observed to depart noticeably from the unperturbed values once secular motion has set in). The examples included in figure 5 also highlight the fact that secular displacement does not necessarily coincide with the time of maximum perturbation amplitude but is rather determined by the fishbone wave frequency (which is linearly swept), so the actual interaction process is still of resonant nature.

To obtain the drop in neutron emission caused by the fishbone, the post-fishbone distribution computed by HAGIS has been inserted again into ASCOT and the volume integrated (D-D) fusion reaction rate re-evaluated, keeping the background profiles fixed. Since for these runs one cannot have additional continuous heating source, it is not possible to directly compare these fusion yields with the steady-state yield presented earlier. Instead, a slowing down calculation has been performed for both the preand the post-fishbone distributions, that is, the slowing of ions is followed for a time interval of 5 ms during which the D-D fusion yield is collected. This approach results in a slightly reduced yield compared to the steady-state yield given earlier but still allows the two cases to be compared. The choice of 5 ms was made as a compromise between minimising statistics noise while still maintaining nearly the same steady state distribution. (The statistics noise was evaluated by running 20 individual simulations each with different random bounce phase, and is here two orders of magnitude lower than the drop magnitude itself.) This neutron rate evaluation has been done for a set of runs with varying fishbone amplitude. The outcome of these computations together with the experimental measurements for an ensemble of 40 fishbones in Pulse No: 69100 (t = 19.6 – 22.3s) is summarised in figure 6. This figure constitutes the main result of this article. For the range of fishbone amplitudes in this discharge, the simulations predict neutron drops of order 0.5 – 1.5%, which increase quadratically with fishbone amplitude. For the experimental data, the drop magnitude has been inferred as follows: The maximum and minimum value of neutron emission signal attained during a fishbone period have been determined and the drop is then defined as the difference between the two, as shown in the figure 6b (an alternative definition using instead the difference in neutron

emission at the beginning and end of a fishbone has also been explored, with very similar results). The error bars on the determination of the fishbone amplitude are dominated by the measurement error of the local temperature gradient prior to the fishbone onset (standard error for the linear fit of four adjacent ECE channels), whereas the vertical error bar is due to the finite noise in the neutron signal. The level of scatter in the experimental data points does not allow for any conclusions to be drawn on whether the amplitude dependence is linear or quadratic, but it can be seen that to within a factor 2 the measured drops are consistent with the simulations. This agreement is very good, especially when considering that it includes three modelling steps from calculating the initial steady state NBI distribution, then applying the FB perturbation with a different code and finally calculating the neutron yield estimation. An important aspect here are also possible changes to the plasma background profiles as a result of the fishbone, and in particular to the plasma background density, as this can have a direct influence onto the newly computed neutron rate. As is shown in figure 1b, which includes a time trace for the central plasma density obtained through Abel inversion of Far-InfraRed (FIR) interferometry measurements, the fishbones (unlike sawteeth) do not have a measurable impact on the plasma density (at least for this particular discharge). From the signal-to-noise ratio of the FIR data, an upper bound for the reduction in central density by the fishbone can be estimated which is in the low sub-percent range. This implies that, by keeping the plasma background density fixed, the effective neutron drop might be underestimated in the simulations by not more than a fraction of a percent, which, when comparing with figure 6, would not impact the level of agreement between experiment and simulation.

CONCLUSIONS

A methodology has been developed to compare fast ion transport in code and experiment in the presence of fishbones. This method complements well code validation attempts with the help of fast ion losses detectors (e.g. 2-D scintillator probe detectors are difficult to get absolutely calibrated). By coupling the HAGIS and ASCOT codes, quantitative predictions on the fast ion redistribution due to fishbones could be made. The codes are found to correctly predict the magnitude of the transient drops in D-D fusion reactivity to within a factor 2. As a next step, a quantitative assessment on whether fishbones will have a sensible impact on ITER's fusion performance (in particular for Operating Scenario 3) is foreseen.

ACKNOWLEDGMENTS

This work was supported by EURATOM and carried out within the framework of the European Fusion Development Agreement. The views and opinions expressed herein do not necessarily reflect those of the European Commission.

REFERENCES

[1]. H.H. Duong et al. Nuclear Fusion, **33**:749, 1993.

[2]. R.B. White et al. Physics of Plasmas, **2**:2871, 1995.

[3]. C.Z. Cheng, L. Chen, and M.S. Chance. Ann. Phys., 161:21, 1985.

[4]. C.Z. Cheng and M. S. Chance. Physics of Fluids, **29**:3695, 1986.

[5]. K.L. Wong. Plasma Physics and Controlled Fusion, **41**:R1, 1999.

[6]. W.W. Heidbrink. Physics of Plasmas, **15**:055501, 2008.

[7]. E.M. Carolipio et al. Physics of Plasmas, **8**:3391, 2001.

[8]. Y. Todo et al. Physics of Plasmas, **10**:2888, 2003.

[9]. W.W. Heidbrink et al. Physical Review Letters, **99**:245002, 2007.

[10]. Y. Todo, H.L. Berk, and B.N. Breizman. Nuclear Fusion, **50**:084016, 2010.

[11]. R.B.White, N. Gorelenkov,W.W. Heidbrink, and M.A. Van Zeeland. Physics of Plasmas, **17**:056107, 2010.

[12]. R. B. White, N. Gorelenkov, W. W. Heidbrink, and M. A. Van Zeeland. Plasma Physics and Controlled Fusion Fusion, **52**:045012, 2010.

[13]. K. McGuire et al. Physical Review Letters, **50**:891, 1983.

[14]. J.D. Strachan et al. Nuclear Fusion, **25**:863, 1985.

[15]. W.W. Heidbrink, R. Hay, and J. D. Strachan. Physical Review Letters, **53**:1905, 1984.

[16]. W.W. Heidbrink et al. Physical Review Letters, **57**:835, 1986.

[17]. R. Kaita et al. Plasma Physics and Controlled Fusion, **28**:1319, 1986.

[18]. W.W. Heidbrink, R. Kaita, H. Takahashi, G. Gammel, G.W. Hammett, and S. Kaye. Physics of Fluids, **30**:1839, 1987.

[19]. P. Smeulders et al. in Controlled Fusion and Plasma Heating (Proc. 17th Eur. Conf. Amsterdam, 1990), Vol. 14B, Part I, European Physical Society, Geneva (1990) 323.

[20]. M.F.F. Nave, D. J. Campbell, E. Joffrin, F. B. Marcus, G. Sadler, P. Smeulders, and K. Thomsen. Nuclear Fusion, **31**:697, 1991.

[21]. M.F.F. Nave et al. in Controlled Fusion and Plasma Heating (Proc. 19th Eur. Conf. Innsbruck, 1992), Vol. 16C, Part I, European Physical Society, Geneva (1992) 136.

[22]. L. Chen, R.B. White, and M.N. Rosenbluth. Physical Review Letters, **52**:1122, 1984.

[23]. B. Coppi and F. Porcelli. Physical Review Letters, **57**:2272, 1986.

[24]. C. Perez von Thun et al. Nuclear Fusion, **50**:084009, 2010.

[25]. C. Perez von Thun et al. Nuclear Fusion, **51**:053003, 2011.

[26]. L.-G. Eriksson, T. Hellsten, and U. Willén. Nuclear Fusion, **33**:1037, 1993.

[27]. J. Hedin, T. Hellsten, L.-G. Eriksson, and T. Johnson. Nuclear Fusion, 42:527, 2002.

[28]. R.J. Goldston, D.C. McCune, H.H. Towner, S.L. Davis, R.J. Hawryluk, and G.L. Schmidt. Journal of Computational Physics, **43**:61, 1981.

[29]. L.C. Appel et al. Nuclear Fusion, **35**:1697, 1995.

[30]. S.D. Pinches et al. Computer Physics Communications, **111**:133, 1998.

[31]. D.W. Roberts et al. Physical Review Letters, **71**:1011, 1994.

[32]. A.B. Mikhailovskii et al. Plasma Physics Report, **23**:844, 1997.

[33]. C.Z. Cheng. Physics Reports, **211**:1, 1992.

[34]. J.A. Heikkinen and S. K. Sipilä. Physics of Plasmas, **2**:3724, 1995.

[35]. R.B. White, R. J. Goldston, K. McGuire, A. H. Boozer, D. A. Monticello, and W. Park. Physics of Fluids, **26**:2958, 1983.

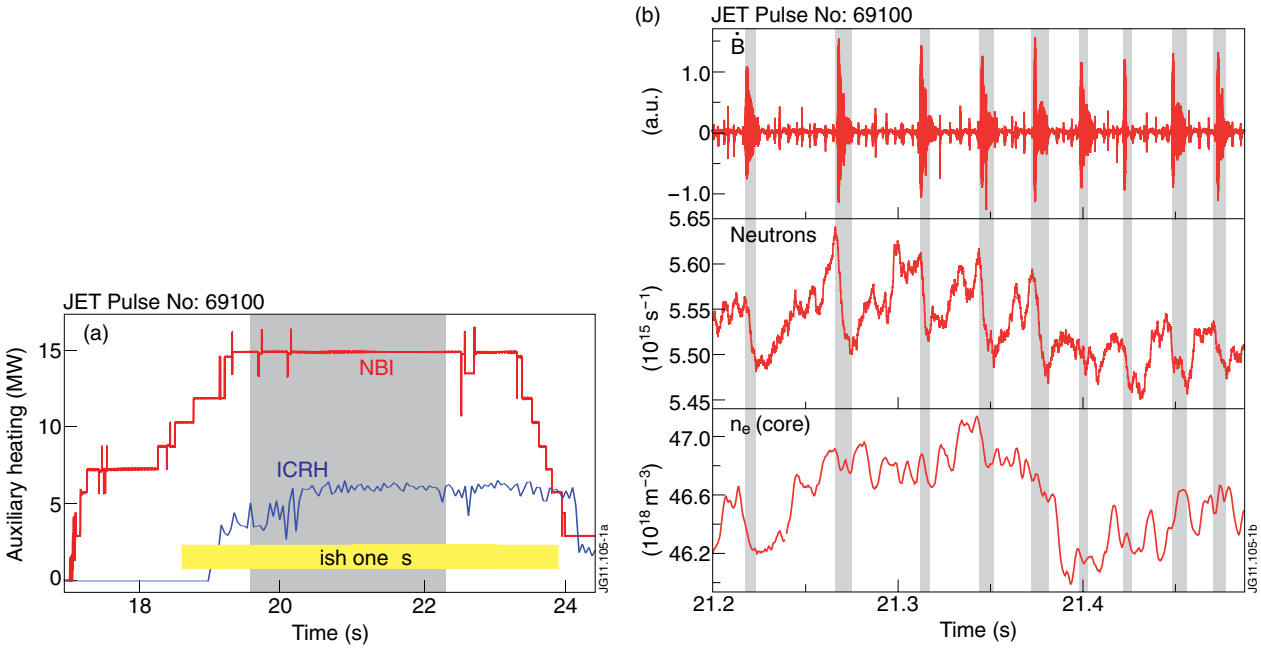

Figure 1: (a) Time traces for neutral beam and ICRH heating in Pulse No: 69100. The yellow box marks the time interval in which fishbones are present. All fishbones used in this paper occur in the time interval 19.57-22.30s (shaded area). (b) Time window of Pulse No: 69100 showing magnetic fluctuations picked up by a Mirnov coil (top), neutron emission from the plasma measured by one of the fission chambers (middle) and time evolution of the central plasma density (inside the q = 1 rational surface at a normalised poloidal flux coordinate ψ = 0.01) (bottom). The latter signal has been obtained from Abel inversion of Far Infrared (FIR) Interferometry signals.

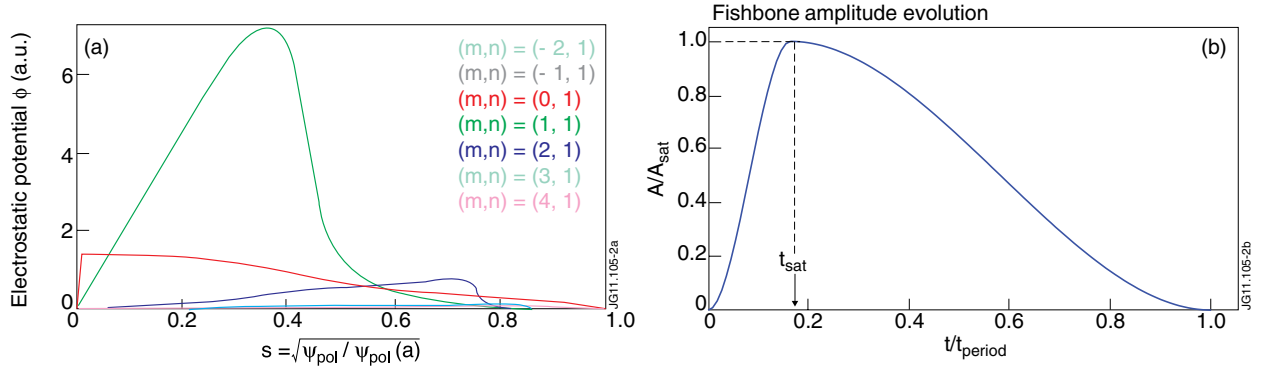

Figure 2: (a) Radial profiles of the electrostatic potential of the n = 1 internal kink perturbation, computed by MISHKA for Pulse No: 69100. The radial coordinate s is the square root of the poloidal magnetic flux. In the legend, $-2 \le m \le 4$ denotes the poloidal harmonic. (b) Waveform of the n = 1 kink amplitude used in HAGIS, including the definitions of the quantities t_{sat}, t_{period} and A_{sat}. $A \equiv \delta\tilde{B}_r/B_0$ is the perturbed radial magnetic field normalised to the magnetic field on axis.

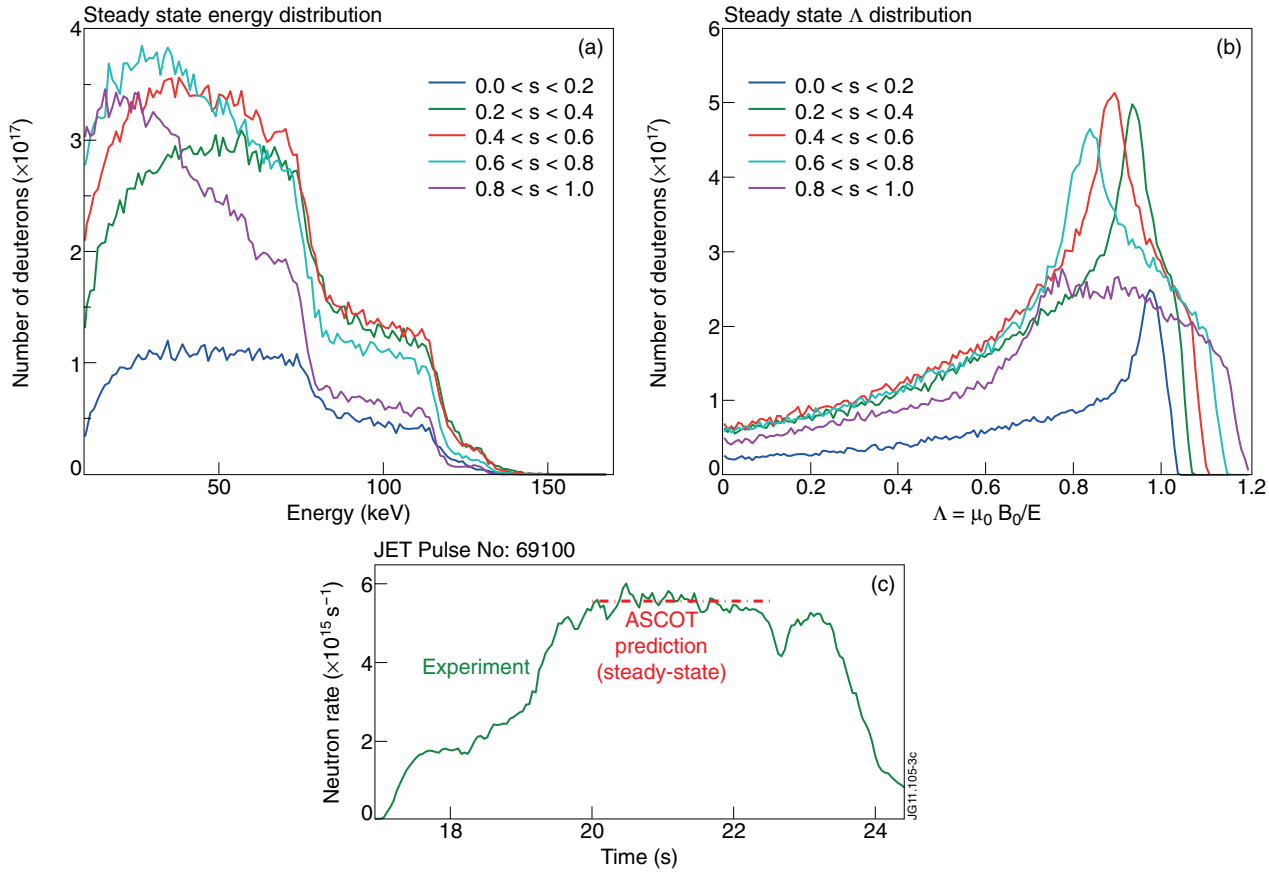

Figure 3: Steady-state slowing down distribution of neutral beam injected fast ions computed by ASCOT for Pulse No: 69100 (a) as a function of energy and (b) as a function of Λ (see text), sliced in radial intervals of $s = \sqrt{\psi_{pol}(r)/\psi_{pol}(a)}$. *(c) Corresponding neutron emission predicted by ASCOT for that distribution together with the experimental measurement.*

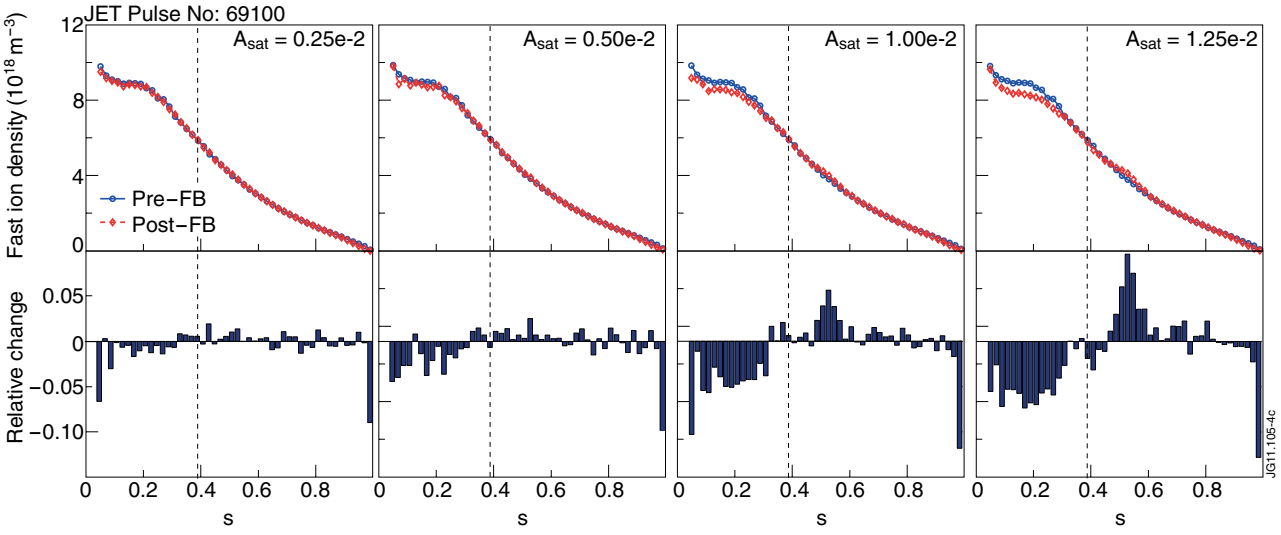

Figure 4. Radial profiles of the absolute fast ion density before and after a fishbone (top row) and the relative change between the two (bottom row) for various fishbone amplitudes (from left to right: $A_{sat} = 2.5 \cdot 10^{-3}$, $5.0 \cdot 10^{-3}$, $1.0 \cdot 10^{-2}$, $1.25 \cdot 10^{-2}$*). The dashed line marks the position of the q = 1 rational surface.*

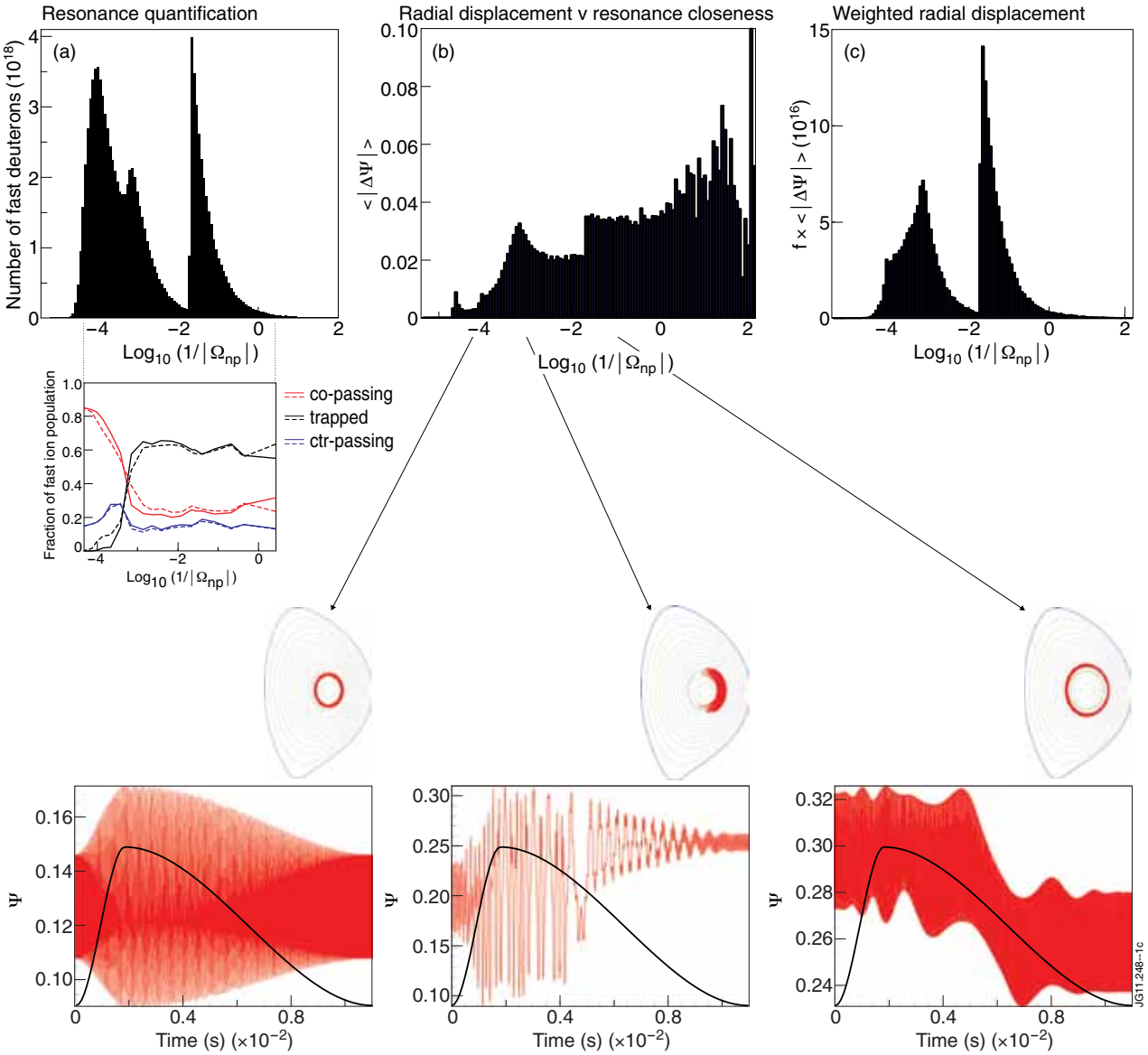

Figure 5: (a) Resonance closeness of the steady-state neutral beam fast ion distribution with respect to the fishbone perturbation wave, expressed in terms of the resonance parameter $log_{10}(|1/\Omega_{np}|)$ (see text). The mixture of orbit types is plotted underneath (solid lines). Also included are the changes to this mixture as a result of a fishbone with amplitude $A_{sat} = 1.0 \cdot 10^{-2}$ (dashed lines). (b) Variation with resonance closeness of the average radial displacement (per ion) induced by the fishbone ($\Delta\Psi$ denotes here the change in normalised poloidal flux of pre- and post-FB orbits after orbit averaging) for a fishbone of amplitude $A_{sat} = 1.0 \cdot 10^{-2}$. Three examples of dynamic orbit behaviours in the presence of the fishbone are shown underneath (resonance parameter increases from left to right), where the overlaid black line indicates the fishbone amplitude throughout the cycle. The left and right hand side examples show two co-passing ions with similar orbit topology, but only the right hand side ion undergoes secular motion due to its higher resonance proximity. Shown in the middle is an example of a perturbed trapped ion. (c) Product of (a) and (b).

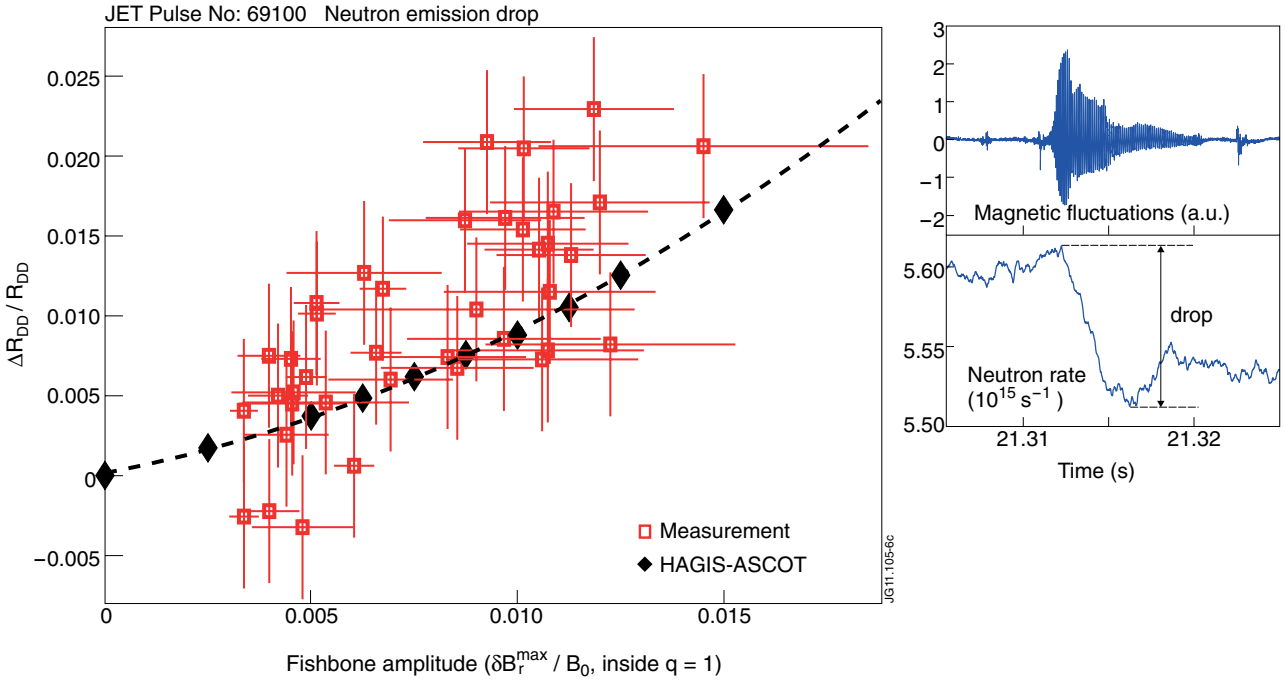

Figure 6: Measured (squares) and simulated (diamonds) drop in volume integrated neutron emission caused by fishbones, as a function of the fishbone amplitude $A_{sat} = \delta B_{r,max}/B_0$. For the experimental data, the value of Asat has been obtained by matching the magnetic flux surface displacement inside q = 1 (visualized through Poincaré plots of magnetic field lines in the 3D perturbed equilibrium) to electron temperature profile displacements measured with an array of ECE radiometers at the time of maximum fishbone amplitude. The figure to the right shows how the measured neutron emission drop has been inferred from the neutron rate signal. For the error bars, see main text.